IEEE Access
Multidisciplinary | Rapid Review | Open Access Journal

Received April 15, 2019, accepted May 5, 2019, date of publication May 23, 2019, date of current version June 3, 2019.

Digital Object Identifier 10.1109/ACCESS.2019.2917514

Morphology-Based Banknote Fitness Determination

S. LEE[1], E. CHOI[2], Y. BAEK[2], AND C. LEE[1], (Member, IEEE)
[1]School of Electrical and Electronic Engineering, Yonsei University, Seoul, South Korea
[2]Advanced Development, Research and Development, Nautilus Hyosung Inc., Seoul, South Korea

Corresponding author: C. Lee (chulhee@yonsei.ac.kr)

ABSTRACT Replacing unfit banknotes is an integral part of maintaining public confidence in currencies while maximizing banknote lifespan in public payment facilities. This paper presents a banknote fitness determination method which mainly focuses on soil and stain detection using images scanned with contact image sensors (CIS). Difference images between fit and unfit banknotes may be used to determine fitness. However, these images may contain erroneous edges since the CIS images usually have some alignment errors caused by scanning, printing, and cutting operations. To resolve this problem, we first categorized the soiling patterns into two types: large- and small-scale. Then we used two different morphological-based methods to eliminate the false edges by security features. After the soiling patterns were extracted, the fitness level was estimated by a maximum standard score. The proposed method showed promising performance when using the Euro and Russian banknote databases.

INDEX TERMS Image processing, image classification, morphological operations, machine learning.

I. INTRODUCTION

Maintaining public confidence in currencies is one of the most important tasks for central banks. Since unfit banknote circulation may negatively affect public confidence, most central banks have set up their own standards for fitness requirements to ensure the integrity and preservation of their currencies. For instance, the European Central Bank (ECB) has adopted minimum standards for euro banknotes, which include several criteria for fitness sorting [20] such as soiling, stains, graffiti, tears, holes, etc. Soiling is mainly caused by aged human sebum and this is considered as one of the main reasons for banknote deterioration [1], [2], [9]. To meet the standards, banknote handling machines have been designed to automatically detect unfit notes. Such machines usually have charge-coupled device (CCD) based image sensors with various wavelengths and thickness detection modules to detect unfit banknotes. Accurate determination of banknote fitness reduces banknote production costs [11] since banknote lifespan can be maximized by recirculating all fit banknotes [6]. Also, automatic replacement of unfit banknotes with new banknotes enables cost-efficient and effective handling by banknote accepting devices in payment facilities such as automatic teller machines (ATM), automatic fare collection machines, retail kiosks, vending machines, etc.

Banknote fitness determination is, however, a challenging problem for commercial cash handlers such as ATMs. Traditionally, banknote fitness has been measured by banknote fitness sorting machines that are expensive and mostly staff-oriented ones [6]. Spectrophotometric devices can also be used to determine banknote fitness by measuring the optical density and comparing it with pre-defined threshold values measured from new and unused banknotes [20]. On the other hand, ATMs typically use contact image sensors (CIS) for banknote scanning and have three potential problems: scanning, printing, and cutting variations. Unlike digital cameras, contact image sensors use line-by-line scanning. Once scanned, banknotes are automatically rotated, de-skewed and cropped [21]. However, even for the same banknote, a scanned image may have a different size each time it is scanned. Moreover, folded or crumpled banknotes are usually horizontally shorter. On the other hand, due to variations in the cutting and printing processes, these problems may not be avoided. Three major production processes are used to print banknotes: offset, intaglio and serial number printing. In the offset printing process, a background design is printed by dry offset on both sides of the sheet simultaneously while some tactile features are printed on sheets during the intaglio printing process. In offset and intaglio printing, multiple bills are

The associate editor coordinating the review of this manuscript and approving it for publication was Naveed Akhtar.

2169-3536 © 2019 IEEE. Translations and content mining are permitted for academic research only.
Personal use is also permitted, but republication/redistribution requires IEEE permission.
See http://www.ieee.org/publications_standards/publications/rights/index.html for more information.

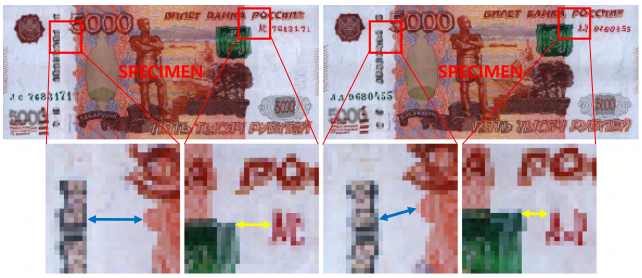

FIGURE 1. Serial numbers and treasury seals are usually printed afterwards, and may have different positions on each note.

printed on a large sheet. For example, 32 individual banknotes are printed on the same sheet in US dollar denominations. However, serial numbers are printed after the sheets are cut into individual banknotes. As shown in Fig. 1, some banknote design elements (seals, serial numbers, main objects, etc.) may end up in slightly different positions if the banknotes are not accurately cut by cutting machines. Thus, banknote images cannot always be accurately aligned, and direct calculation of difference images between two banknotes may result in unwanted edges around dominant features. For ATMs with limited computing power, computational complexity is also an important factor for algorithm development since typical ATMS should be able to handle about 10 banknotes per second or more. Thus, a fast banknote fitness determination method is desirable, which can be applied to scanned images where accurate image registration methods may not be available.

In this paper, two morphology-based methods are proposed, which extract two kinds of soiling patterns: large- and small-scale patterns (Fig. 2). Soiled banknotes usually have soiling across the whole banknote, whilst stained banknotes have locally concentrated soiling. These large-scale patterns are easily identifiable if the banknote images are aligned well enough for the difference images to be calculated. By using closed difference images (CDI), we tried to bypass the alignment errors by removing the banknote features that shifted in position. On the other hand, soiled banknotes also have small-scale soiling patterns due to intaglio printing and banknote circulation. Since elevated edges or points are more likely to be soiled with fingerprints than dented surfaces, soiled banknotes usually have fold lines along with speckle patterns [8]. Those are usually in small-scale and appear as dark patterns. We used a generalized dynamic morphological difference image (GDMDI) to extract such patterns, which is a modified version of GDMQI [13]. In this method, alignment errors can be ignored since strong edges can be suppressed with GDMDI. Thus the resulting image does not contain unwanted features such as serial numbers. We extracted large- and small-scale soiling patterns as images for each side and each channel (R, G and B) of banknote scanned images, and then the averages and standard deviations were used for banknote fitness determination. Combining these two methods allowed us to obtain favorable performance when using EUR and RUB databases.

FIGURE 2. Soiling pattern extraction examples of (a) fit banknote and (b) unfit banknote. From the first to fifth row: Original, morphologically closed, modified dynamic closed, large-scale soiling pattern, small-scale soiling pattern images.

II. PREVIOUS WORKS

In recent studies, researchers explored to use region of interests (ROI) suitable for detecting dirt. Balke *et al.* used a machine learning method to select such regions [3]. Using training data fit and unfit banknotes, they first extracted statistical values from pre-defined regions. For each region, a simple threshold-based classifier was trained with the extracted values. Instead of using all the classifiers, they applied the Adaptive Boosting method [7] to select relatively stronger classifiers than the others. On the other hand, Kwon *et al.* manually selected a fixed homogeneous ROI and used discrete wavelet transformation to extract features [10]. These methods are, however, not available for newly designed banknotes. In other words, the two-class classifiers cannot be applied when only fit banknotes are available. Also, the classifier may be prone to overfitting if there are not enough unfit banknotes. Moreover, local dirt cannot be detected when it is outside the selected regions.

In our preliminary work [12], we proposed two different methods for soiled banknote fitness determination. One was a morphology-based method and the other was based on the Otsu threshold method [18]. In the morphology-based method, a selective closing operation was used. Since folded lines or edges are usually soiled by human fingerprints, we tried to extract these patterns using morphological operations. However, conventional closing operations also remove serial numbers and other intricate banknote features. If a pixel shown on the closed image is larger than the corresponding

pixel of the original image by a given threshold, the original pixel is retained. Otherwise, the pixel of the closed pixel is used. If the threshold is small, only small points or edges can be removed.

On the other hand, banknotes may also show discoloring, which is mainly caused by microorganisms [4]. Discolored banknotes usually have lower dynamic ranges than new banknotes. Thus, we developed an Otsu-based method to estimate the discolor level. A pixel was first classified as a background or foreground pixel using the Otsu threshold. Then, we estimated the banknote soiling level by computing the average pixel intensities of the background and foreground pixels. However, only the green channel images of the front side of banknotes were used in [12]. In this case, it is difficult to detect green-color soiling.

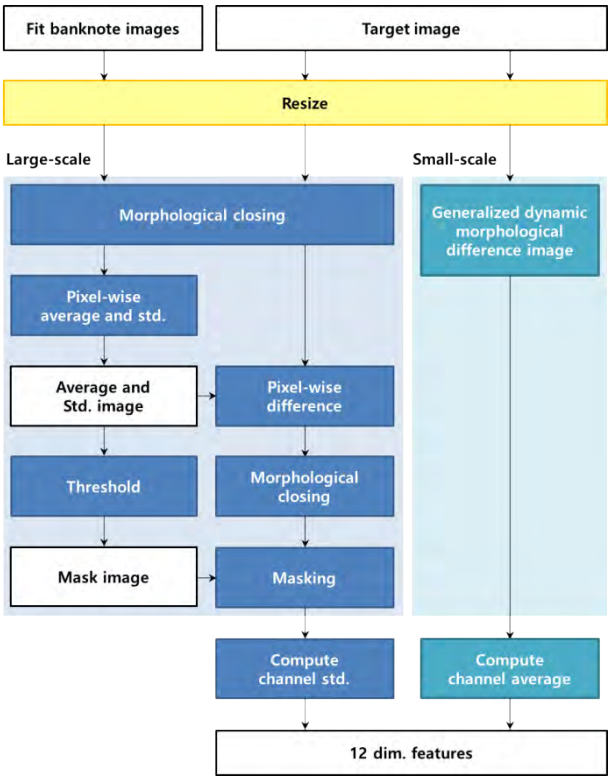

FIGURE 3. Flow chart of soiling pattern and feature extraction.

III. METHODOLOGY

In this section, three main processing steps will be described in detail: large- and small-scale soiling pattern extraction, feature extraction and fitness determination. Using these steps, we aim to detect various types of soiling and estimate banknote fitness from the soiling pattern images. Fig. 3 shows detailed steps of the soiling pattern and feature extraction process. The large-scale soiling pattern extraction process requires fit banknotes as references for comparison whereas small-scale soiling extraction does not.

A. A LARGE-SCALE SOILING PATTERN EXTRACTION

An effective way to extract soiling patterns is to compute difference images using fit banknotes. To obtain meaningful difference images, two images need to be aligned. Feature-based image registration techniques (e.g. SIFT[15], SURF[5], BRISK[14]) are usually time-consuming and control point-based methods require manual selection. Also, printed features such as serial numbers are likely to be misaligned, as illustrated in Fig. 2. In other words, erroneous edges may still appear in the difference images even if the images are globally aligned. To resolve this problem, we removed the erroneous edges by applying a morphological closing operation as a preprocessing step. Closing makes small holes and dark narrow lines filled with the values of their neighboring pixels. Since the printed features are usually printed with dark ink, the closing operation can effectively remove them.

In general, banknote fitness determination methods need to be developed by using only reference banknotes since all soiling patterns may not be available. Moreover, unfit banknote samples may not exist for newly designed banknotes. Thus we used only reference images of fit banknotes for algorithm development. First, we generated a preprocessed fit banknote image as follows:

$$\hat{I}_f = I_f \bullet T_{u\times u} \tag{1}$$

where I_f represents a resized fit banknote image and $\bullet$ denotes the morphological closing operation with the structuring element $T_{u\times u}$. Note that all banknote images were first resized to the average width W and height H. Each banknote contained six different color channels (2 sides $\times$ 3 channels (RGB)). For each channel, we computed the average and standard deviation images μ and σ as follows:

$$\mu(x,y) = \frac{1}{N}\sum_{N} I_{f,n}(x,y) \tag{2}$$

$$\sigma(x,y) = \sqrt{\frac{1}{N}\sum_{N} I_{f,n}^2(x,y) - (\mu(x,y))^2} \tag{3}$$

where N represents the number of fit banknote images and $(x,y) \in R^{W\times H}$. For a target banknote image I_t, a large-scale soiling pattern image (Z_t) was computed as follows:

$$Z_t(x,y) = \frac{I_t(x,y) - \mu(x,y)}{\sigma(x,y)}, \tag{4}$$

which is known as data whitening. Note that $Z_t(x,y)$ tends to be negative in the bright regions since soiled or stained banknotes are usually darker than reference banknotes. Since $Z_t(x,y)$ can be negative, we made some brightness level adjustments based on the histograms. Figs. 4(b–c) show the following image, $Z_t'(x,y) = 5Z_t(x,y) + 255$. As can be seen in Fig. 4(b), erroneous edges appeared around dominant objects due to local alignment errors. To reduce these erroneous edges, we applied a morphological closing operation to Z_t:

$$\hat{Z}_t(x,y) = \frac{\{I_t(x,y) - \mu(x,y)\} \bullet T_{u\times u}}{\sigma(x,y)} \tag{5}$$

We will call $\hat{Z}_t$ as closed difference image (CDI). Fig. 4(c) shows that the morphological closing operation effectively

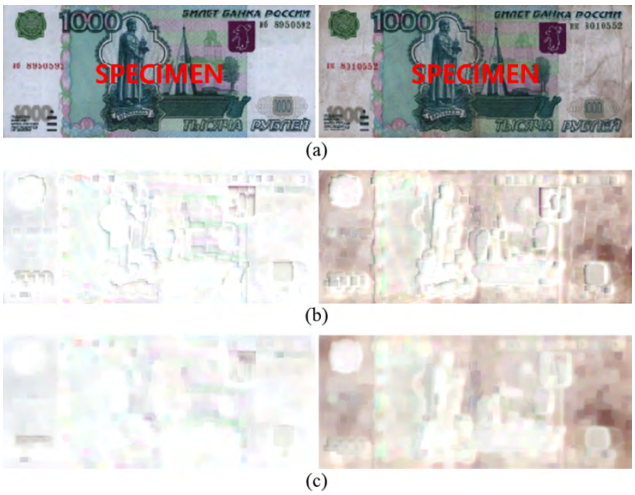

FIGURE 4. Fit (left) and unfit banknote images (right). (a) Russian RUB 1000 CIS banknote images. (b) The large-scale soiling pattern images show alignment errors. (c) The alignment errors were reduced with morphological operations. Note that the intensity levels of the large-scale soiling pattern images were adjusted to [0–255].

reduced the erroneous edges. For strong alignment errors, masking operations were used. The pixel intensities around the dominant object boundaries fluctuated greatly and showed large standard deviations. Thus, we used thresholded standard deviation images as masking images.

B. SMALL-SCALE SOILING PATTERN EXTRACTION

As stated in SectionI, elevated edges or points are more likely to be soiled with aged human sebum [1]. Such protruding regions can be produced in two ways: intaglio printing and banknote seals. Intaglio printing is a widely-used security printing technique. This process requires a metal plate on which pre-designed images are engraved. First, the engraved regions are filled with ink. Then, the ink is transferred to the sheet at high pressure, and at the same time, the inked region rises slightly compared to the adjacent regions. Thus, intaglio printing features are tactile [19]. Whereas these tactile features are made by printing machines, crumples and folds are usually made during circulation. Such wrinkles are often difficult to reverse since banknotes usually lose their stiffness once they are folded [2]. Compared to the large-scale soiling patterns, speckles and fold lines are relatively small and narrow in size. Such small-scale soiling patterns can be easily eliminated using morphological closing operations. However, these operations also may remove other dark, small and narrow banknote features. As can be seen in Fig. 5(b), the edges of serial numbers, denomination numbers, letters and object boundaries are strong and the influence of small-scale soiling patterns is relatively small after the closing operation.

To solve this problem, the closing operation needs to be selectively applied to preserve strong edges so that different images have soiling patterns only. One possible solution is to use the generalized dynamic morphological quotient image (GDMQI) [13], a multiscale morphology-based method, which was first introduced for face illumination compensation. For face images, bright light sources may produce strong edges (shadows) on face surfaces. One of the main concerns for most illumination compensation methods is to eliminate the effect of shadows. In this context, the GDMQI method can take advantage of the edge-preserving property of multiscale morphological operations [13], [16], [17], whereas other methods suffer from halo effects that usually occur around the shadow regions. The GDMQI is defined as follows:

$$\rho(x,y) = C_l(x,y)/C_s(x,y) \tag{6}$$

$$P(x,y) = 1/\left[1+\exp\{-k(\rho(x,y)-\gamma)\}\right] \tag{7}$$

$$GDC(x,y) = C_l(x,y)P(x,y) + C_s(x,y)\{1-P(x,y)\} \tag{8}$$

$$GDMQI(x,y) = I(x,y)/GDC(x,y) \tag{9}$$

where GDC denotes generalized dynamic closing, and C_l and C_s are two different closing images obtained by using large ($l \times l$) and small ($s \times s$) structuring elements, respectively. Note that ρ and P are intermediate images. GDMQI's edge-preserving property can also be used for maintaining banknote features if soiling patterns are eliminated. However, the GDMQI method cannot be directly applied to this problem since it is based on the Retinex theory. According to this theory, an observed image can be modeled as a product of an illumination image and a reflectance image. This is why the ρ value and the GDMQI image are based on division operations. On the other hand, unfit banknote images cannot be decomposed into illumination and reflectance images. Instead, we considered the small-scale soiling patterns as additive noise. Thus, we rewrote eq. (6–9), and defined a generalized dynamic morphological difference image (GDMDI) as follows:

$$\rho'(x,y) = C_l(x,y) - C_s(x,y) \tag{10}$$

$$P'(x,y) = 1/\left[1+\exp\left\{-k\left(\rho'(x,y)-\gamma\right)\right\}\right] \tag{11}$$

$$MGDC(x,y) = C_l(x,y)P'(x,y) + C_s(x,y)\left\{1-P'(x,y)\right\} \tag{12}$$

$$GDMDI(x,y) = MGDC(x,y) - I(x,y) \tag{13}$$

Simply, the MGDC image can be interpreted as a blend function between two closing images C_l and C_s. More specifically, if $\rho(x,y) > \gamma$ and $k > 0$, then $P'(x,y) > 0.5$ and C_l is dominant. If C_l removes dark, small and narrow objects while C_s preserves them, $\rho(x,y) > \gamma$. Since our target is to preserve such objects, k should be negative here. Figs. 5(c-d) show some examples of the GDMQI and GDMDI results. Small-scale soiling patterns were successfully extracted by the GDMQI method, though denomination numbers and some strong edges were still visible. On the other hand, most banknote features (seals, serial numbers, main objects, etc.) were removed by the GDMDI method (Fig. 5(d)).

C. FEATURE EXTACTION AND BANKNOTE FITNESS DETECTION

Each scanned banknote has two RGB images: front and back sides. Thus there were six channels. We applied the CDI and GDMDI methods independently to each channel, and obtained six CDIs and six GDMDIs per banknote. For the 12 channels, we computed average pixel intensity values, and constructed a 12-dimensional vector v as follows:

$$v = \frac{1}{WH}\left[\sum_{y=1}^{H}\sum_{x=1}^{W}\hat{Z}_{t,1}(x,y), \sum_{y=1}^{H}\sum_{x=1}^{W}\hat{Z}_{t,2}(x,y), \cdots, \sum_{y=1}^{H}\sum_{x=1}^{W}\hat{Z}_{t,6}(x,y), \cdots \sum_{y=1}^{H}\sum_{x=1}^{W}GDMDI_1(x,y), \sum_{y=1}^{H}\sum_{x=1}^{W}GDMDI_2(x,y), \cdots, \sum_{y=1}^{H}\sum_{x=1}^{W}GDMDI_6(x,y)\right]^T \quad (14)$$

where $\hat{Z}_{t,i}(x,y)$ and $GDMDI_i$ represent the CDI and GDMDI of the i-th channel, respectively.

Instead of using the full images, we only used the vectors to reduce computation complexity. CDI methods are generally used for extracting large-scale soiling patterns: soiling on the entire banknote and locally concentrated soiling. Using average values is not helpful to find locally concentrated soiling. If the area of local soiling is small (e.g. 10×10 pixels), the average value of the extracted soiling pattern image will also be small. In this case, standard deviations might provide more discriminative power for banknote fitness detection. As can be seen in Fig. 4(c), extracted soiling patterns of fit banknotes are usually low in value (Note that the images in Fig. 4(c) are inverted images). Thus, their standard deviations are also low whereas banknotes with soiling have larger standard deviations.

On the other hand, the average intensity values of GDMDIs also provide useful information for soiling detection. As shown in Fig. 5(d), GDMDIs have many micro patterns designed for security in addition to small-scale soiling patterns. However, this is not a critical issue if we use averages. Whereas fit banknotes contain micro patterns, soiled banknotes may contain both micro patterns and soiling patterns. This might cause the average values of unfit banknotes to be higher than those of fit banknotes.

For banknote fitness determination, we designed the classifier by considering the following. First, as stated in Section II.A, we regarded banknote fitness determination as a single class classification since we did not have sufficient prior knowledge of soiling patterns, particularly for newly designed banknotes. Second, we aimed to minimize the computational complexity since the computation power of typical ATMs is moderate and commercial ATMs need to process at least 10 banknotes per second. Lastly, soiling patterns of

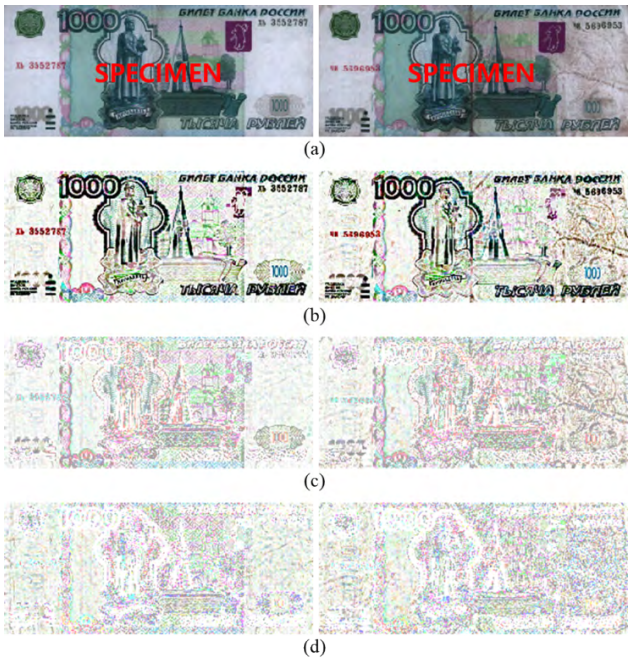

FIGURE 5. (a) Fit (left) and unfit (right) Russian RUB 1000 CIS banknote images. (b) Difference between original and closed images. (c) Generalized dynamic morphological quotient images (GDMQI) and (d) generalized dynamic morphological difference images (GDMDI). Note that (b-d) are inverted images.

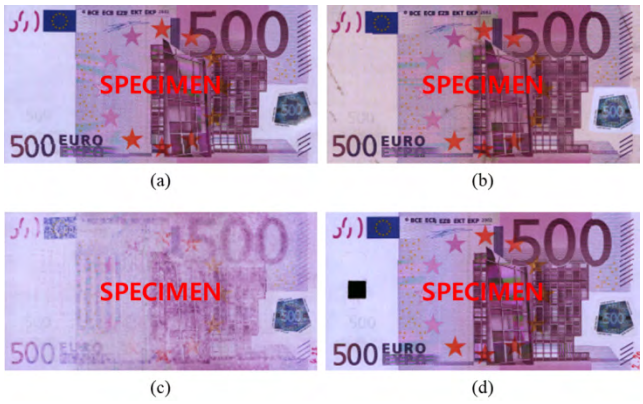

FIGURE 6. Some EUR 500 banknote examples of banknote databases. (a) A fit banknote. Unfit banknotes: (b) soiled, (c) de-inked and (d) stained.

any RGB channels had to be detected and such banknotes had to be classified as unfit banknotes. With the aforementioned considerations, we selected reference banknotes (i.e. fit banknotes) and computed the mean and standard deviation of the feature vectors as the reference mean vector $\mathbf{m}$ and the reference standard deviation vector $\mathbf{s}$. Then we developed a maximum standard score (MSS) to estimate the banknote fitness levels:

$$MSS(\mathbf{x}) = \max\left(\left(x_i - m_i\right)/s_i\right) \quad (15)$$

where x_i represents the i-th element of vector $\mathbf{x}$. m_i and s_i denote the i-th element of $\mathbf{m}$ and $\mathbf{s}$. As explained in Section III.B, the x_i values of unfit banknotes were larger

TABLE 1. Number of fit and unfit banknotes and equal error rates (%) obtained by different methods on euro banknotes (EUR).

Denomination	5	5	10	10	20	20	50	100	200	500
Issued Year	2002	2013	2002	2014	2002	2015	2002	2002	2002	2002
# Fit	120	120	128	163	152	147	179	61	104	120
# Unfit_Soil	36	32	33	35	33	3	33	33	33	33
# Unfit_De-ink	8	10	10	8	10	2	10	10	10	14
# Unfit_Stain	36	30	33	26	33	3	33	33	33	33
# Total	200	192	204	232	228	155	255	137	180	200
Average [12]	33.75	31.94	28.95	27.61	26.32	37.50	48.04	31.58	31.58	17.50
Sobel edge [12]	27.50	15.28	15.79	32.52	10.53	12.50	15.79	21.05	35.53	27.50
Otsu + Selective [12]	1.67	0	1.32	10.14	6.58	0.68	12.32	5.26	2.63	0
GDMDI	36.25	40.28	36.84	27.54	28.95	12.50	34.64	26.23	31.58	22.50
CDI	0	0	0	0	0	0	0	0	0	0
GDMDI+CDI	0	0	0	0	0	0	0	0	0	0

TABLE 2. Number of fit and unfit banknotes and equal error rates (%) obtained by different methods on russian banknotes (RUB).

Denomination	50	100	500	500	1000	1000	5000	5000
Issued Year	2004	2004	2004	2010	2004	2010	1997	2010
# Fit	360	1200	1200	1200	1216	1200	1600	1600
# Unfit	800	800	465	120	604	796	800	264
# Total	1160	2000	1665	1320	1820	1996	2400	1864
Average [12]	0	0	0	0	3.31	0.50	0.25	10.61
Sobel edge [12]	0	1.00	7.76	10.00	23.18	6.68	11.75	39.39
Otsu + Selective [12]	0	0	0	0	1.97	0.50	0.25	3.03
GDMDI	0	0	0	0	1.97	0.67	0.25	6.50
CDI	0	0	0	0	1.99	0.50	0	0
GDMDI+CDI	0	0	0	0	1.32	0.50	0	0

than those of the fit banknotes. Also, the max(·) operation was used to find the largest difference. Then, *MSS* (**x**) was used to represent the fitness level. By using the reference banknotes, one can calculate their maximum MSS value as a threshold for classifying unfit banknotes.

IV. EXPERIMENTS

A. DATABASES

Contact image sensor images of real banknotes (50 dots per inch (DPI)) were used in the experiments. We used both sides of the RGB images. There were 12 different denominations from the EU and Russian banknotes: Euro (EUR: 5, 10, 20, 50, 100, 200, 500) and Russian Ruble (RUB: 50, 100, 500, 1000, 5000). Some denominations feature two different designs (EUR: 5, 10, 20, and RUB: 500, 1000, 5000) and so there were a total of 18 different designs. Tables 1 and 2 show the number of fit and unfit banknotes. The unfit EUR banknotes consisted of three categories: soiled, de-inked, and stained. Fig. 6 shows some examples of fit and unfit banknotes. The soiled EUR banknotes were usually soiled across the entire region. For the de-inked EUR banknotes, the entire banknotes were discolored. Also, the stained EUR banknotes had a stamp mark (a black square). On the other hand, the unfit RUB banknotes have no category classification, though most of them were soiled banknotes. Also, some stained banknotes were included in the RUB 1000 denominations (2014).

B. EXPERIMENTAL RESULTS

Tables 1 and 2 also show the banknote fitness determination results. For each denomination, the fitness levels of the banknotes were first computed and sorted. Then we computed the equal error rates (EER: the false rejection rate and the false acceptance rate are identical) using the receiver operation characteristic (ROC) curve, which was used for performance comparison. To compare the proposed method (GDMDI + CDI) with other methods, we also tested the following: average pixel intensity (Average) [12], average pixel intensity of a Sobel operator applied image (Sobel edge) [12], and a combination of Otsu-based and selective closing (Otsu + Selective) [12]. We also provided the results when either GDMDI or CDI were used. For all the denominations, we used fixed parameters: $k = -5$, $\gamma = 22$, $l = 5$ and $s = 1$, for the GDMDI method. These parameters were

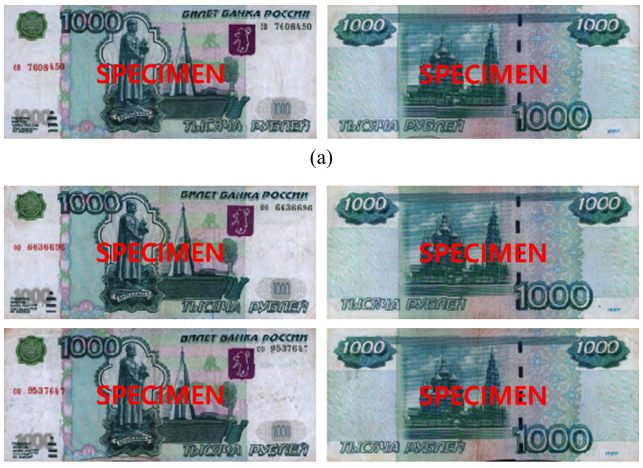

(a)

(b)

FIGURE 7. (a) A fit RUB 1000 banknote. (b) Unfit RUB 1000 banknotes erroneously classified as fit.

empirically determined based on the EUR 5 fit banknotes. In all the denominations, the combined method (GDMDI + CDI) showed the best performance. Using only the GDMDI method was not good for EUR banknote fitness determination. As can be seen in Table 2, the average pixel intensity value may be a good and simple solution since the average intensity values of soiled notes are usually lower than those of fit ones. However, this method may fail for de-inked or stained banknotes. For example, soiled EUR notes were perfectly classified for all denominations whereas the error rates of the de-inked and stained notes were 93.48% (86/92) and 43.00% (128/293), respectively. We used the EER threshold values, obtained from the ROCs. The combined method (GDMDI + CDI) showed errors of about 1.32% for the RUB 1000 (2004 and 2010) banknotes. As can be seen in Fig. 7, the soiling level of the error banknotes (unfit banknotes) was very low, which indicates the proposed method was able to accurately predict the soiling level of the banknotes.

V. CONCLUSIONS

In this paper, we proposed a banknote fitness determination method. We first classified the soiling patterns into two types: large- and small-scale soiling patterns. Then, we used two different morphology-based banknote fitness determination methods. The CDI method was developed to extract large-scale soiling patterns, which required fixed size reference images. Also, the GDMDI, a modified version of the GDMQI method [13], was proposed to capture the small-scale soiling patterns. By combining these two methods, we developed a method that showed promising results for banknote databases that contained 18 different designs of EUR and RUB banknotes. Especially, the proposed methods successfully detected the soiling patterns of the unfit RUB banknotes.

REFERENCES

[1] P. Balke, "New soiling test method: Anti-dirty fingers," De Nederlandsche Bank, Amsterdam, The Netherlands, Tech. Rep., 2009.
[2] P. Balke, "From fit to unfit: How banknotes become soiled, Watermark," De Nederlandsche Bank, Amsterdam, The Netherlands, Tech. Rep., 2011.
[3] P. Balke, J.-M. Geusebroek, and P. Markus, "BRAIN2—Machine learning to measure banknote fitness," in *Proc. Opt. Document Secur. Conf.*, Jan. 2012, pp. 18–20.
[4] W. J. Bartz and T. T. Crane, "Circulation simulator method for evaluating bank note and optical feature durability," *Proc. SPIE.*, vol. 6075, Feb. 2006, Art. no. 607505.
[5] H. Bay, A. Ess, T. Tuytelaars, and L. Van Gool, "Speeded-up robust features (SURF)," *Comput. Vis. Image Understand.*, vol. 110, no. 3, pp. 346–359, 2008.
[6] H. Deinhammer and A. Ladi, "Modelling euro banknote quality in circulation," Eur. Central Bank, Frankfurt, Germany, Tech. Rep. 204, 2017.
[7] Y. Freund and R. E. Schapire, "A decision-theoretic generalization of on-line learning and an application to boosting," *J. Comput. Syst. Sci.*, vol. 55, no. 1, pp. 119–139, Aug. 1997.
[8] J.-M. Geusebroek, P. Markus, and P. Balke, "Learning banknote fitness for sorting," in *Proc. Int. Conf. Pattern Anal. Intell. Robot.*, Jun. 2011, pp. 41–46.
[9] E. Kropnick, "Measurement of banknote soiling by sorting machines: An empirical study," *Billetaria-Int. Rev. Cash Manage.*, vol. 11, pp. 24–26, Apr. 2012.
[10] S. Y. Kwon, T. D. Pham, K. R. Park, D. S. Jeong, and S. Yoon, "Recognition of banknote fitness based on a fuzzy system using visible light reflection and near-infrared light transmission images," *Sensors*, vol. 16, no. 6, p. 863, Jun. 2016.
[11] N. M. Lawandy and A. Y. Smuk, "Supercritical fluid cleaning of banknotes," *Ind. Eng. Chem. Res.*, vol. 53, no. 2, pp. 530–540, Dec. 2013.
[12] S. Lee, S. Baek, E. Choi, Y. Baek, and C. Lee, "Soiled banknote fitness determination based on morphology and Otsu's thresholding," in *Proc. IEEE Int. Conf. Consum. Electron. (ICCE)*, Jan. 2017, pp. 450–451.
[13] S. Lee and C. Lee, "Multiscale morphology based illumination normalization with enhanced local textures for face recognition," *Expert Syst. Appl.*, vol. 62, pp. 347–357, Nov. 2016.
[14] S. Leutenegger, M. Chli, and R. Y. Siegwart, "BRISK: Binary robust invariant scalable keypoints," in *Proc. Int. Conf. Comput. Vis. (ICCV)*, Nov. 2011, pp. 2548–2555.
[15] D. G. Lowe, "Object recognition from local scale-invariant features," in *Proc. 7th IEEE Int. Conf. Comput. Vis.*, Sep. 1999, pp. 1150–1157.
[16] S. Mukhopadhyay and B. Chanda, "An edge preserving noise smoothing technique using multiscale morphology," *Signal Process.*, vol. 82, no. 4, pp. 527–544, Apr. 2002.
[17] S. Mukhopadhyay and B. Chanda, "Multiscale morphological segmentation of gray-scale images," *IEEE Trans. Image Process.*, vol. 12, no. 5, pp. 533–549, May 2003.
[18] N. Otsu, "A threshold selection method from gray-level histograms," *IEEE Trans. Syst., Man, Cybern.*, vol. 9, no. 1, pp. 62–66, Jan. 1979.
[19] K. Springer, P. Subramanian, and T. Turton, "Australian banknotes: Assisting people with vision impairment," *Bull. Reserve Bank Aust*, vol. 2015, pp. 1–12, Mar. 2015.
[20] F. van der Horst, M. Eschelbach, S. Sieber, and J. Miedema, "Does banknote quality affect counterfeit detection? Experimental evidence from Germany and the Netherlands," *Jahrbücher für Nationalökonomie und Statistik*, vol. 237, no.6, pp. 469–497, Dec. 2017.
[21] S. Youn, E. Choi, Y. Baek, and C. Lee, "Efficient multi-currency classification of CIS banknotes," *Neurocomputing*, vol. 156, pp. 22–32, May 2015.